In-situ SAXS/WAXS investigations of ureidopyrimidinone functionalized semi-crystalline poly(ethylene-co-butylene) supramolecular polymers

Maroua Louati, Jean-Francois Tahon, David Fournier, Grégory Stoclet,
Stéphane Aloïse, Marumi Takao, Michinori Takeshita, Jean Marc Lefebvre,
Sophie Barrau

In-situ SAXS/WAXS investigations of ureidopyrimidinone functionalized semi-crystalline poly(ethylene-co-butylene) supramolecular polymers

Maroua Louati,[1,2,3] Jean-François Tahon,[1] David Fournier,[1] Gregory Stoclet,[1] Stéphane Aloise,[2] Marumi Takao,[3] Michinori Takeshita,[3] Jean-Marc Lefebvre[1] and Sophie Barrau,[1,*]

[1] Université de Lille, CNRS, INRAE, Centrale Lille, UMR 8207 - UMET - Unité Matériaux Et Transformations, F-59000 Lille, France

[2] Université de Lille, CNRS, UMR 8516 - Lasir - Laboratoire de Spectrochimie Infrarouge et Raman, F-59000 Lille, France

[3] Department of Advanced Technology and Fusion, Graduate School of Science and Engineering, University of Saga, Japan

[*] Corresponding author. E-mail address: sophie.barrau@univ-lille.fr (S. Barrau)

Abstract

The structural evolution as a function of temperature of a supramolecular copolymer assembly based on multiple hydrogen bonds has been investigated. Ureidopyrimidinone functionalized semi-crystalline poly(ethylene-co-butylene) (PEB-(L-UPy)$_2$) has been characterized by means of in situ WAXS and SAXS experiments. The crystallinity and the nature of crystal forms are associated to the ethylene sequences. Special attention has been paid to the impact of the hydrogen bonding network on the structural arrangements, by comparison to the unfunctionalized PEB. The presence of crystalline domains of in-plane arrangement between neighboring UPy dimers is detected by WAXS up to 80°C. The SAXS data reflect the presence of L-UPy aggregates stable on the whole temperature range. The correlation of these UPy-based aggregates is effective until the PEB crystal melting temperature (Tm). Beyond Tm, the increase of the macromolecular mobility reduce the number of domains in interaction and, in consequence, implies a decorrelation of the aggregates.

Keywords: supramolecular polymer, hydrogen bonds, ureidopyrimidinone (UPy), correlation distance, crystal phase, SAXS

1. Introduction

Supramolecular polymers (SMPs) are defined as polymers generated through non-covalent interactions of entities such as monomers, oligomers or polymers as well. Owing to the non-covalent bond reversibility, supramolecular polymers generally display better solubility and processability than commonly used thermoplastic polymers. These non-covalent bonds may imply electrostatic, van der Waals or donor-acceptor interactions, as well as hydrogen bonding.

SMPs based on multiple hydrogen bonds have raised considerable interest.[1, 2] Indeed, the latter provide higher strength and control of directionality by comparison to single hydrogen bonds. In this respect, the self-associating ureidopyrimidinone (UPy) motif via quadruple hydrogen bonds has been extensively used as a linker for the design of supramolecular polymers.[3, 4] UPy functionalization has been reported for a broad panel of polymers including polypropylene,[5] polycaprolactone,[6, 7] polystyrene,[8] polycarbonate,[9] poly(L-lactic acid),[10] polyurethane,[11] polydimethylsiloxanes,[12] poly(ethylene-co-butylene)[13]... Poly(ethylene-co-butylene) (PEB) is a copolymer that displays a degree of crystallinity strongly dependent on the ratio of ethylene to butylene moieties. To sum up, above a 50% butylene content, the copolymer remains amorphous while below this value PEB is semi-crystalline.[14] Investigations on UPy functionalized PEB have mainly focused on amorphous PEB and the resulting supramolecular thermoplastic elastomers. The design of such UPy-based supramolecular thermoplastic elastomers is for instance strikingly exemplified in the work of Meijer et al.[15] who reported the formation of nanofibers due to the lateral aggregation of UPy-urea functions and the stacking of UPy dimers. From Wide-Angle X-ray Scattering (WAXS) profiles, two characteristic distances were evidenced: a hydrogen bonding distance of 0.455 nm found in supramolecular bisurea polymers between stacked urea hydrogen bonds [16] and an in-plane distance of 1 nm between neighboring UPy dimers.[15] Complementary to WAXS information, Small-Angle X-ray Scattering (SAXS) is a powerful tool allowing to probe nano-sized objects or domains. For supramolecular structures, SAXS profile classically reveals a maximum interpreted as the result of a microphase separation between the amorphous polymer matrix and the ordered structure of the functional groups.[17, 18] Indeed, for PEB-UPy, Chang et al.[19] observed a scattering peak corresponding to an average distance of 6.5 nm and associated to the microphase separation from the PEB matrix of UPy dimeric moieties, which form hard domains via the hydrogen bonding interactions.

In the case of semi-crystalline (co)polymers, the physical properties are highly dependent on the crystallinity and the nature of the crystal phase. The crystallinity of PEB is associated to the ethylene sequences. The polymer crystal forms are thus those of poly(ethylene) (PE) with two main crystal forms at atmospheric pressure: the most stable orthorhombic form and the monoclinic form usually obtained under stress such as uniaxial compression.[20-23] The monoclinic form transforms into the orthorhombic form by annealing.[24] The polymer crystal forms are therefore dependent on the film processing history. For the UPy functionalized semi-crystalline copolymer, a competition is expected to occur between the intrinsic trend of organization of the macromolecules into crystals and the self-assembly via hydrogen bonding.

In this context, the present work is dedicated to the understanding of the structure of ureidopyrimidinone functionalized semi-crystalline poly(ethylene-co-butylene) copolymers. Two different elaboration processes (drop casting and film cooling from the melt) have been retained for thin film elaboration. The main objectives are to identify the effect on polymer crystal forms involved and to highlight the hydrogen bonding network signature by means of WAXS and SAXS experiments. The in-situ temperature investigation (below and above the polymer crystal melting) allows to probe the structural evolution of the thin film with special focus on the impact of UPy functionalization of the PEB.

2. Experimental section

2.1. Materials

Poly(ethylene-co-1,2-butylene)diol (PEB) was purchased from Sigma-Aldrich (M_n ~ 2,500 g/mol). 2-amino-4-hydroxy-6-methylpyrimidine (Tokyo Chemical Industry Co. Ltd), hexamethylene diisocyanate (Tokyo Chemical Industry Co. Ltd), dibutyltin dilaurate (Wako Pure Chemical Industries, Ltd.), methanol (Laboratoire Verbièse), hexane (Laboratoire Verbièse) were used without further purification. Chloroform (Laboratoire Verbièse) was distilled before use.

2.2. Synthesis
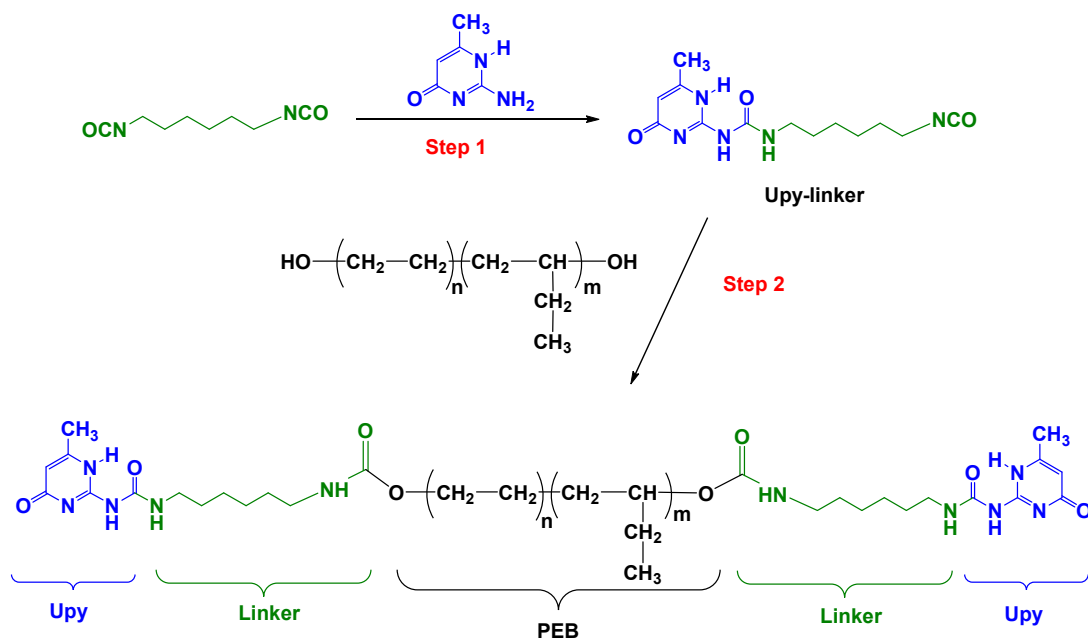
Scheme 1: Synthesis of the UPy-linker (step 1) and telechelic PEB-(L-UPy)₂ (step 2).

2.2.1. UPy-linker

The synthesis of the UPy-linker[25] is reported in Scheme 1 (step 1). The 2-amino-4-hydroxy-6-methylpyrimidine (4 g, 32.1 mmol) was dissolved in hexamethylene diisocyanate (25 g, 150 mmol) under argon atmosphere. The reaction mixture was heated at 100°C in an oil bath overnight. A stepwise cooling approach was employed to slowly cool the solution down to room temperature. The collected residue was washed intensively with hexane and then dried at 50°C under vacuum, resulting in a white solid (9.0g, 30.7 mmol, yield: 95.6%). NMR spectrum is presented in Figure S1.

2.2.2. Telechelic UPy-functionalized PEB (called PEB-(L-UPy)₂)

The UPy-functionalized PEB was synthesized according to literature (Scheme 1 - step 2).[6, 13] Briefly, a solution of UPy-linker (9.0g, 30.7 mmol) and poly(ethylene-co-1,2-butylene)diol (19 g, 7.5 mmol), dibutyltin dilaurate (0.1 ml) and chloroform (250 ml) was stirred for 24h at 60°C under argon. To remove the excess of UPy-linker, 4g of Silica beads and 0.1 mL of dibutyltin dilaurate were added. After 2h at 60°C, the silica was removed by filtration and the chloroform was removed using rotary evaporator. The UPy-functionalized PEB was further dried under vacuum at 50°C for 2 days (white solid, 8.3g). NMR spectra of commercial PEB and PEB-L-UPy are reported in Figure S2. From the NMR spectrum of commercial PEB diol in CDCl₃, the molar fractions of ethylene and butylene could be estimated to 87% and 13% respectively.

2.3. Film preparation

Two procedures were followed to assess the impact of the processing route. Telechelic PEB-(L-UPy)$_2$ copolymer was dissolved in chloroform at 60°C for 1h under gentle magnetic stirring to allow the connection of UPy end-groups. For the first route, the solution was drop cast on glass plates and then dried under vacuum at room temperature. The obtained drop cast thin film is labeled as PEB-(L-UPy)$_2$ DC. For the second route, once the evaporation was achieved for the drop cast solution, the film was melted at 170°C and then cooled down at a cooling rate of around 10°C/min. The obtained thin film is referred to as PEB-(L-UPy)$_2$ CM. The thickness of the films obtained by both methods is around 100 µm. Note that the reference PEB film was obtained under conditions similar to those for PEB-(L-UPy)$_2$ DC.

2.4. Methods

Thermal characterization of the polymers was achieved on a DSC-Q20 Perkin-Elmer instrument calibrated according to standard procedures using a high purity indium sample. For the analyses, samples (5 - 10 mg) were placed into aluminum pans and heated from ambient temperature to 170°C at a rate of 10°C/min under nitrogen atmosphere. The sample crystallinity was calculated according to equation (1):

$$\chi_c = \frac{\Delta H_m}{\Delta H_m^0} \qquad (1)$$

where ΔH_m is the enthalpy of fusion and ΔH_m^0 is the enthalpy of fusion of 100% crystalline polyethylene, $\Delta H_m^0 = 293$ J.g^{-1}.[26, 27]

Wide angle X-ray scattering (WAXS) and Small-angle X-ray scattering (SAXS) experiments were carried out on a Xeuss 2.0 (Xenocs) operating under vacuum with a GeniX3D microsource ($\lambda = 1.54$ Å) at 0.6 mA and 50 kV and a 2D Pilatus 3R 200K detector. Analyses were performed in transmission mode. The WAXS patterns were acquired with a sample-to-detector distance of 160 mm while the SAXS detector was positioned at 2300 mm from the sample. From the patterns, WAXS and SAXS scattered intensities were integrated and plotted against the scattering angle 2θ and the scattering vector, $q = (4\pi/\lambda)\sin\theta$, respectively. For the in-situ experiments as a function of temperature, a Linkam hot-stage was used. The thin films were heated from ambient temperature to 170°C by step of 5 or 10°C. The acquisition time is 600s. Peak fit® software was used for diffractogram deconvolution by using a combination of Gaussian and Lorentzian functions. For the modeling of the SAXS profiles, the "Irena macro" software running under Igor Pro was used.[28] As discussed in the next section two scattered

populations have been considered for the modeling. On the hand the stacked PEB crystalline lamellae embedded into the PEB amorphous matrix and on the other hand the UPy dimers. For both a them the scattering profile have been modeled using a unified model for the form factor and an interference model for the structure factor.[29, 30]

3. Results and discussion

3.1. WAXS experiments

Considering the high ethylene content as indicated by NMR analysis, crystallization of PEB is expected. The structure of PEB and PEB-(L-UPy)$_2$ was characterized by WAXS in order to identify the polymer crystal phases and to probe the signature of the SMP assembly. The WAXS pattern of PEB (not shown) reveals the presence of two rings, indicative of an isotropic distribution of the crystalline lamellae.
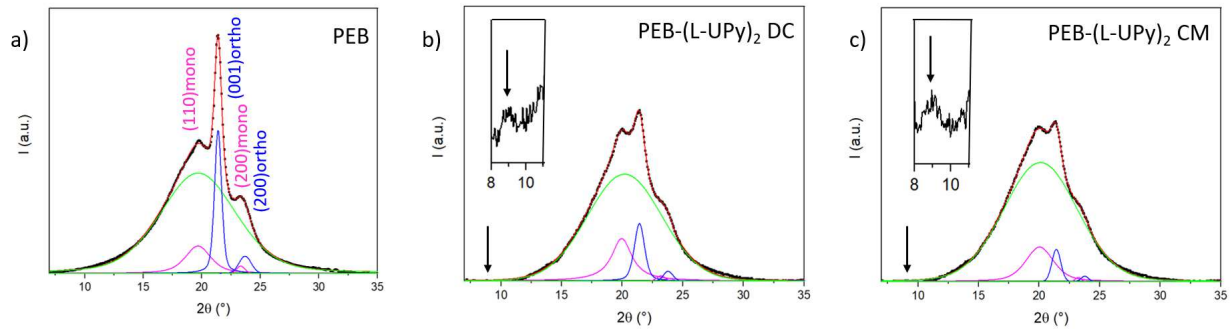

Figure 2: WAXS intensity profiles and deconvolution of a) PEB, b) PEB-(L-UPy)$_2$ DC and c) PEB-(L-UPy)$_2$ CM, the peak corresponding to the PE orthorhombic and monoclinic forms are in magenta and blue respectively. The insets show the peak at $2\theta = 8.7°$ attributed to the reflection of crystalline UPy domains.

The integrated intensity profile of PEB (Figure 2a) displays different peaks. The WAXS spectra was fitted to extract the fractions of amorphous and crystalline phases and to define the polymer crystal form. The deconvolution of the intensity profile shows the presence of four peaks embedded in a large halo characteristic of an amorphous fraction. The two main peaks at $2\theta = 21.2°$ and $2\theta = 23.5°$ correspond to the (110) and (200) planes of the orthorhombic form of PE (a = 7.40 Å, b = 4.93 Å, c = 2.54 Å).[24] Two supplementary peaks are observed at $2\theta = 19.5°$ and $2\theta = 23.2°$ and are associated to the (001) and (200) planes of the monoclinic form of PE (a = 8.09 Å, b = 4.79 Å, c = 2.53 Å and $\beta = 107,9°$).[22, 31] Therefore, PEB displays two crystal forms, the orthorhombic and monoclinic forms of PE. The crystallinity and the relative fractions of the two crystal phases are calculated from the

6

peak areas (Table 1). The overall degree of crystallinity is around 22% with a higher fraction of PE orthorhombic. In ethylene copolymers, several studies report the coexistence of the monoclinic crystal form with the orthorhombic crystal form.[32-34] For instance in ethylene-butylene copolymers, Hu et al.[32] report the presence of the monoclinic form in ethylene copolymers with high comonomer content (> 9 mol%) and bulky side groups. The coexistence of the two crystalline forms results from the distribution of ethylene sequences within the copolymer. The longer ethylene sequences crystallize into the orthorhombic form while shorter sequences are in favor of the monoclinic form. Formation of the monoclinic form may also be induced by the cooling rate during crystallization from the melt.

Table 1. Crystallinity (χ), relative fraction (F) of orthorhombic and monoclinic forms, melt temperature (T_m), melt enthalpy (ΔH_m) and long period (L_p) of PEB and PEB-(L-UPy)$_2$ DC and PEB-(L-UPy)$_2$ CM

	$\chi(\%)^1$	F_{ortho} $(\%)^1$	F_{mono} $(\%)^1$	T_m $(°C)^2$	ΔH_m $(J.g^{-1})^2$	$\chi(\%)^2$	L_p $(nm)^3$
PEB	22	60	40	62	61	21	8,9
PEB-(L-UPy)$_2$ DC	21	39	61	53	57	20	8,9
PEB-(L-UPy)$_2$ CM	14	24	76	68	33	12	11,8

[1]from WAXS intensity profile deconvolution, [2]from DSC thermograms, [3]from modelling of SAXS profiles

The WAXS intensity profiles and deconvolutions of PEB-(L-UPy)$_2$ DC and PEB-(L-UPy)$_2$ CM are presented in Figure 2b and Figure 2c. The four peaks previously described are observed but with different intensities. The resulting crystallinity and the relative fraction of the two PE crystal forms are reported in Table 1. The crystallinity of PEB-(L-UPy)$_2$ DC is quasi similar to that of PEB. The main difference is related to the relative fractions of the crystal forms. Indeed, the orthorhombic form is predominant in PEB contrary to PEB-(L-UPy)$_2$ DC where a monoclinic form is prevailing. Considering the thin film preparation in similar conditions for both PEB and PEB-(L-UPy)$_2$ DC, the difference in crystal form fractions may therefore be correlated to the impact of the presence of the L-UPy end groups on the macromolecular chain arrangement. Thermal treatment has as well a significantly impact. Indeed, the PEB-(L-UPy)$_2$ CM sample cooled from the melt at moderate cooling rate

(10°C/min) displays higher relative fraction of monoclinic form and lower crystallinity. Therefore, the polymer crystallization during the cooling results in the formation of crystals in the less stable crystal form. For this sample, the UPy network is expected to constraint the PEB macromolecular chains which induces the formation of the PEB monoclinic form and slightly increases the fraction of amorphous content. A similar evolution of the crystal form and amorphous content has already been report on stretched polyethylene. [31]

A small peak is also observed for both PEB-(L-UPy)$_2$ films at $2\theta = 8.7°$ (black arrow in Figure 2b and 2c) and corresponds to the reflection reported for in-plane crystalline UPy domains (d = 1.0 nm).[7, 35] The second reflection attributed to the interplanar distance between UPy motifs and classically observed at $2\theta = 19.5°$ (d = 0.455 nm) is not visible here probably due to the contribution of PEB crystals in this scattering range.

The in-situ evolution of the WAXS intensity profiles in the temperature range from 30°C to 170°C are presented in Figure 3. The high temperature limit was chosen considering the degradation temperature (T_d) measured by thermo-gravimetric analysis (TGA spectra not shown) for PEB ($T_d = 186\pm1°C$) and for telechelic PEB-(L-UPy)$_2$ ($T_d = 197\pm1°C$).

At the early stages of the temperature rise, the characteristic peaks of both PEB crystal forms decrease due to gradual crystal melting. At 60°C, the main peak attributed to the PE monoclinic form ($2\theta = 19.5°$) disappear. Beyond 90°C, the crystals, in orthorhombic form ($2\theta = 21.2°$), have fully melted. The melting of the less stable monoclinic form then occurrs at lower temperature compared to the orthorhombic form.[36] The small peak observed for both PEB-(L-UPy)$_2$ at $2\theta = 8.7°$ disappears in the vicinity of 80°C (Figure 3d) indicative of the melt of the in-plane crystalline UPy domains at this temperature which is in the temperature range already reported for other UPy-based SMPs.[7, 37]
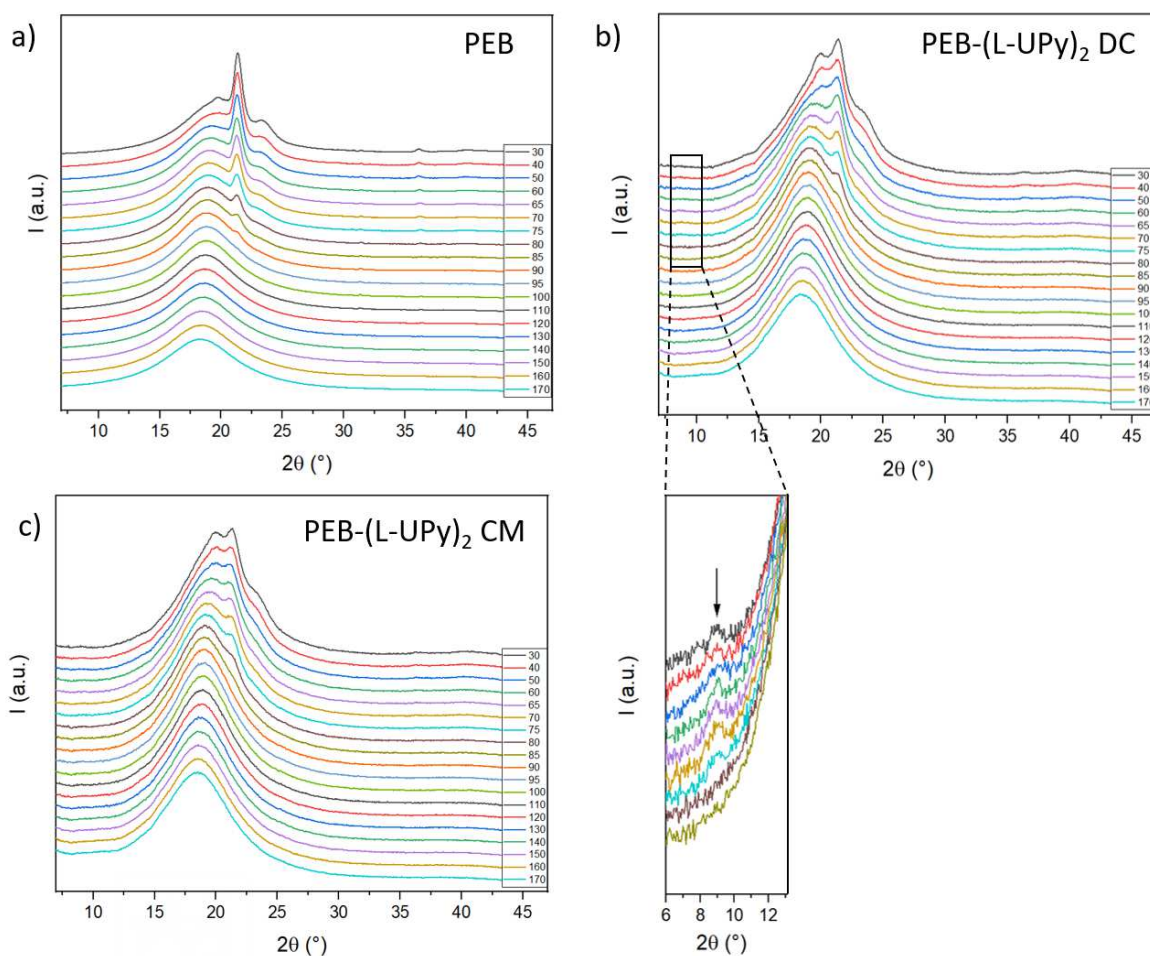
Figure 3: WAXS profiles in-situ in temperature (step of 5 or 10°C) for a) PEB, b) PEB-(L-UPy)$_2$ DC and c) PEB-(L-UPy)$_2$ CM. The inset is a zoom of the peak at $2\theta = 8.7°$ attributed to the reflection of crystalline UPy domains.

The thermal behavior was also probed from DSC measurements. As shown in Figure 4 two main thermal transitions are clearly observed. The first transition is an endothermic step around -25°C associated to the glass transition of the copolymer. At higher temperature, multiple endothermic peaks characteristic of the melting transition appear in the temperature range from 20°C to 90°C. A broad endotherm is usually observed in the random copolymers.[38] In the case of PEB, it can be associated to the melting in distinct temperature ranges of both PE crystals forms,[14] different sizes of crystallites, the co-existence of distinct superstructures...[39, 40] The melting temperatures, the enthalpy values and the resulting crystal content are reported in Table 1.
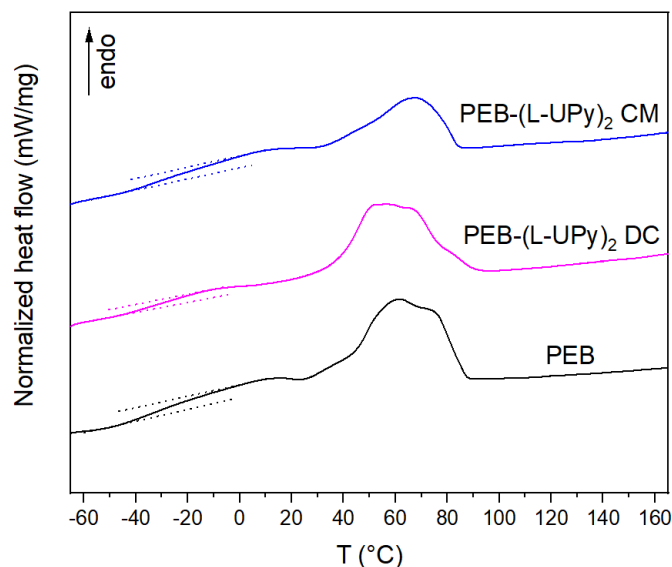
Figure 4: DSC thermograms of PEB, PEB-(L-UPy)₂ DC and PEB-(L-UPy)₂ CM.

Note that the crystal content was derived from the fusion enthalpy of the 100% orthorhombic form. The degree of crystallinity calculated from DSC thermograms is very close to the value reported from WAXS profile deconvolution. The thin film process impacts the position and the width of the endotherms. The melting of the monoclinic form occurring at lower temperature compared to the orthorhombic form, as previously observed, the endothermic peak is not significantly correlated to the melt temperature of both PE crystals forms but rather indicates a broad crystal thickness distribution. The melt temperature is higher for the PEB-(L-UPy)$_2$ CM sample suggesting an increase in crystal thickness for the film crystallized during cooling from the melt.

3.2. SAXS experiments

SAXS experiments are reported at T = 30°C in Figure 5. The SAXS profile of PEB exhibits a main scattering peak associated to the presence of nanoscale arrangements commonly attributed in the case of semi-crystalline polymers to the regular stacking of the crystalline lamellae into the amorphous matrix. The position of the scattering maxima allows to define the long-period (L_p) which corresponds to the characteristic distance of the regular stacking of amorphous and crystalline fractions. For both PEB-(L-UPy)$_2$ samples, the SAXS profile is more complex and exhibits two peaks. The behavior will be addressed on the basis of the temperature evolution results in the following part.
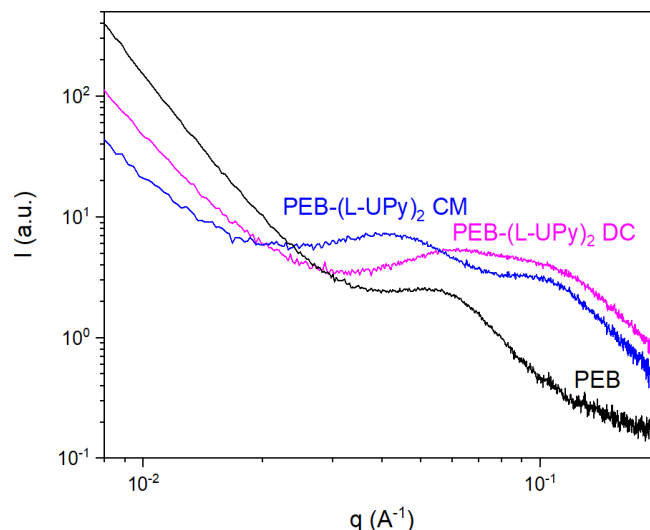
Figure 5: SAXS scattering profiles of PEB, PEB-(L-UPy)$_2$ DC and PEB-(L-UPy)$_2$ CM at T=30°C.

In-situ SAXS experiments have been performed as a function of temperature from 30°C to 170°C. The SAXS profiles of PEB, presented in Figure 6a, show a shift of the main scattering peak at lower q. The PEB long-period reported versus the temperature in Figure 7a then increases up to PE crystal melting.[41] Above the melt temperature (T > 90°C), L_p disappears. As expected the SAXS data for PEB are in agreement with the DSC thermogram previously described (Figure 4).

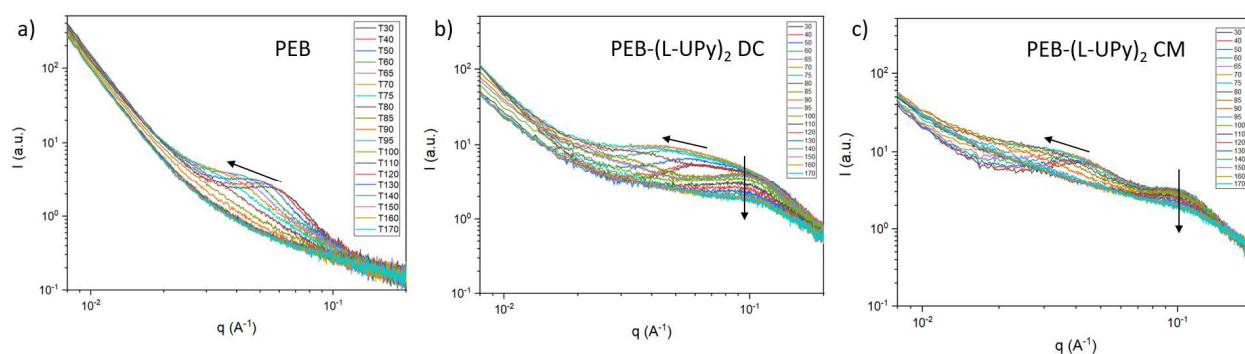*Figure 6: SAXS scattering profiles in temperature (step of 5 or 10°C) of a) PEB, b) PEB-(L-UPy)$_2$ DC and c) PEB-(L-UPy)$_2$ CM.*

Both PEB-(L-UPy)$_2$ samples (Figure 6b and Figure 6c) display similar behavior. Starting from 30°C, the lowest q-contribution shifts to lower values in the temperature range from 30 to 90°C, while the highest q-contribution remains quasi-constant over the whole temperature range. The lowest q-contribution then corresponds to the increase of the PEB L_p up to crystal

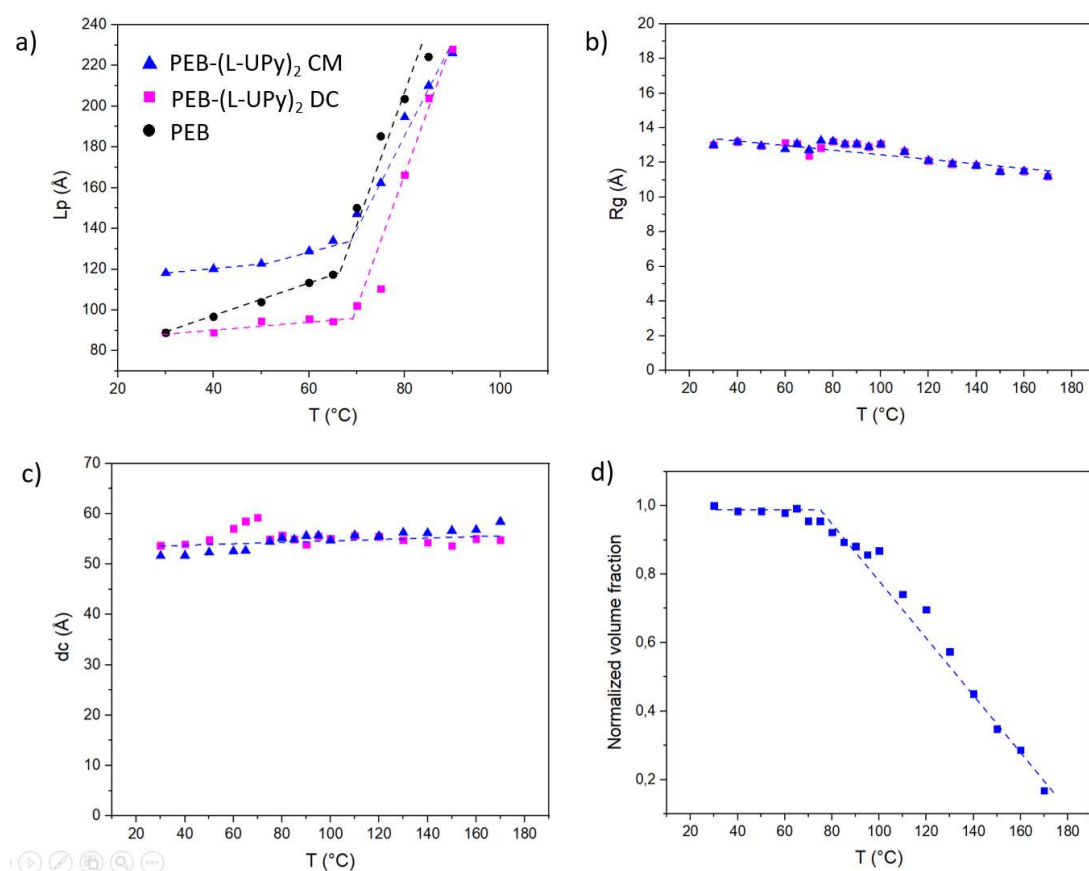melting and the highest q-contribution seems attributed to the presence of UPy-based diffusing objects.

Figure 7: Parameters obtained from the SAXS profiles modeling: a) the long period (L_p) of PEB, b) the gyration radius (Rg), c) the correlation distance (dc) and d) the normalized volume fraction of PEB (black circles), PEB-(L-UPy) DC (pink squares) and PEB-(L-UPy) CM (blue triangle up).

Modeling of the SAXS profiles was undertaken in order to extract the characteristics features of the systems (Figure S2). For both PEB-(L-UPy)$_2$, the evolution of the lower-q contribution, i.e. the PEB L_p, and the higher-q contribution, i.e. the gyration radius (Rg), the correlation distance (dc) and the normalized volume fraction are reported in Figure 7. At ambient temperature, the values of L_p are highly sensitive to the process used for thin film preparation (Figure 7a). L_p of PEB and PEB-(L-UPy)$_2$ DC are similar (around 9 nm) while L_p of PEB-(L-UPy)$_2$ CM is significantly higher (11.8 nm). For this latter, the increase of the long period is in accordance with the increase in crystal thickness previously mentioned. Nevertheless, the temperature evolution is similar for the two PEB-(L-UPy)$_2$ samples, L_p is quasi-constant from 30 to 65°C and then significantly increases from the temperature of the crystal melting (observed by DSC in Figure 4 and reported in Table1) until the complete melt at around 90°C.

Worth mentioning, the PEB L_p starts to increase from ambient temperature, indicative of an instable morphology while PEB-(L-UPy)$_2$ maintains a stable supramolecular assembly until either the melt of the crystalline UPy domains such as in-plane crystalline domains observed by WAXS at 80°C or the melt of PEB crystals. The UPy domains contribution at $2\theta = 8.7°$ being highly negligible compared to the signature of PEB crystal forms (Figure 2), the change of behavior is correlated to the melt of this latter.

For UPy-based diffusing objects, the Rg values comprised between 11 and 13 Å (Figure 7b) remain quasi constant over the whole temperature range. Considering that the UPy-based scatters have a disk shape (due to the fact that a slope close to -2 was found with the unified fit), the diameter of the resulting diffusive domains, calculated from the relation $D = 2R = 2Rg\sqrt{1/2}$, is comprised between 15 and 19 Å. This domain size is higher than the size of UPy dimer (diameter around 13 Å [42]) and may correspond to diffusive L-UPy aggregates, i.e. domains including UPy dimers but as well aggregates of urethane (L-groups) hydrogen bonding. The correlation distance between two diffusive domains (Figure 7c) from 50 to 55 Å is attributed to the distance between two L-UPy aggregates. The independence of this parameter with the temperature displays the interaction between diffusing domains is possible on the whole temperature range but a change of the dc volume fraction may be expected. The evolution of the normalized volume fraction (Figure 7d) is quasi constant until the melt of PEB crystals. Above Tm a linear decrease is observed until a fraction of 17%. The mobility released by the PEB melt reduce the number of domains in interaction probably due to the increase of molecular mobility with the increase of the temperature.

From these experiments, two main arrangements are highlighted for both PEB-(L-UPy)$_2$ samples: (i) the presence of PEB crystals is observed from ambient temperature up to PEB crystal melting at 90°C and (ii) the signatures of the UPy interactions, namely the presence of crystalline domains of in-plane arrangement between neighboring UPy dimers is slightly detected up to 80°C, and L-UPy aggregates are observed on the whole temperature range up to 170°C. Interestingly, although melting of PEB is achieved, the UPy functionalized polymers are still connected via hydrogen bonds of UPy end groups, the latter being known to present a high association constant (K = 6.10^7 M^{-1} in chloroform).[25] However the correlation distance between domains of L-UPy aggregates is significantly impacted by the PEB melt temperature. Finally, in such system, not only the UPy interactions but as well the PEB crystals contribute to maintain a stable morphology.

4. Conclusions

This work focuses on the structural evolution with temperature of supramolecular polymers based on multiple hydrogen bonds. PEB end-functionalized with UPy-motifs (PEB-(L-UPy)$_2$), able to self-assemble via quadruple hydrogen bonding moieties, were successfully synthesized. The signature of different PE crystal forms was clearly identified. The PEB-(L-UPy)2 copolymer presents a high fraction of the monoclinic PE crystal form in addition to the usual orthorhombic form, depending on the thin film thermal treatment. In-situ scattering experiments enabled to emphasize the temperature evolution of well-defined structural arrangements. At ambient temperature, the presence of crystalline domains of in-plane arrangement between neighboring UPy dimers is observed. The UPy-based aggregates present a stable morphology until the PEB crystal melting temperature (Tm). Above PEB melting, the morphology is impacted by the macromolecular mobility which reduce the number of domains in interaction and, in consequence, implies a decorrelation of the aggregates. These supramolecular copolymers could further be used as macromolecular backbones in the design of photoactivable systems, for instance, photomechanical SPMs based on UPy functionalized photochromic molecules [43] and semi-crystalline polymer relying on quadrupole hydrogen bonding.

References

[1] W.H. Binder, R. Zirbs, Supramolecular Polymers and Networkswith Hydrogen Bonds in the Main- and Side-Chain, in: W. Binder (Ed.), Hydrogen Bonded Polymers, Springer Berlin Heidelberg, Berlin, Heidelberg, 2007, pp. 1-78.
[2] L. Bouteiller, Assembly via Hydrogen Bonds of Low Molar Mass Compounds into Supramolecular Polymers, in: W. Binder (Ed.), Hydrogen Bonded Polymers, Springer Berlin Heidelberg, Berlin, Heidelberg, 2007, pp. 79-112.

[3] M. Wubbenhorst, J.v. Turnhout, B.J.B. Folmer, R.P. Sijbesma, E.W. Meijer, Complex dynamics of hydrogen bonded self-assembling polymers, IEEE Transactions on Dielectrics and Electrical Insulation 8(3) (2001) 365-372.

[4] R.P. Sijbesma, F.H. Beijer, L. Brunsveld, B.J.B. Folmer, J.H.K.K. Hirschberg, R.F.M. Lange, J.K.L. Lowe, E.W. Meijer, Reversible Polymers Formed from Self-Complementary Monomers Using Quadruple Hydrogen Bonding, Science 278(5343) (1997) 1601-1604.

[5] S. Nojiri, H. Yamada, S. Kimata, K. Ikeda, T. Senda, A.W. Bosman, Supramolecular polypropylene with self-complementary hydrogen bonding system, Polymer 87 (2016) 308-315.

[6] D.J.M. van Beek, A.J.H. Spiering, G.W.M. Peters, K. te Nijenhuis, R.P. Sijbesma, Unidirectional Dimerization and Stacking of Ureidopyrimidinone End Groups in Polycaprolactone Supramolecular Polymers, Macromolecules 40(23) (2007) 8464-8475.

[7] J.-L. Wietor, D.J.M. van Beek, G.W. Peters, E. Mendes, R.P. Sijbesma, Effects of Branching and Crystallization on Rheology of Polycaprolactone Supramolecular Polymers with Ureidopyrimidinone End Groups, Macromolecules 44(5) (2011) 1211-1219.

[8] K. Yamauchi, J.R. Lizotte, D.M. Hercules, M.J. Vergne, T.E. Long, Combinations of Microphase Separation and Terminal Multiple Hydrogen Bonding in Novel Macromolecules, Journal of the American Chemical Society 124(29) (2002) 8599-8604.

[9] P.Y.W. Dankers, Z. Zhang, E. Wisse, D.W. Grijpma, R.P. Sijbesma, J. Feijen, E.W. Meijer, Oligo(trimethylene carbonate)-Based Supramolecular Biomaterials, Macromolecules 39(25) (2006) 8763-8771.

[10] J. Bao, X. Chang, Q. Xie, C. Yu, G. Shan, Y. Bao, P. Pan, Preferential Formation of β-Form Crystals and Temperature-Dependent Polymorphic Structure in Supramolecular Poly(l-lactic acid) Bonded by Multiple Hydrogen Bonds, Macromolecules 50(21) (2017) 8619-8630.

[11] J. Rong, J. Zhong, W. Yan, M. Liu, Y. Zhang, Y. Qiao, C. Fu, F. Gao, L. Shen, H. He, Study on waterborne self-healing polyurethane with dual dynamic units of quadruple hydrogen bonding and disulfide bonds, Polymer 221 (2021) 123625.

[12] N.E. Botterhuis, D.J.M. van Beek, G.M.L. van Gemert, A.W. Bosman, R.P. Sijbesma, Self-assembly and morphology of polydimethylsiloxane supramolecular thermoplastic elastomers, Journal of Polymer Science Part A: Polymer Chemistry 46(12) (2008) 3877-3885.

[13] H.M. Keizer, R. van Kessel, R.P. Sijbesma, E.W. Meijer, Scale-up of the synthesis of ureidopyrimidinone functionalized telechelic poly(ethylenebutylene), Polymer 44(19) (2003) 5505-5511.

[14] C.A. Sierra, C. Galan, J.G. Fatou, M.D. Parellada, J.A. Barrio, Thermal and mechanical properties of poly (styrene-b-ethylene-co-butylene-b-styrene) triblock copolymers, Polymer 38(17) (1997) 4325-4335.

[15] W.P.J. Appel, G. Portale, E. Wisse, P.Y.W. Dankers, E.W. Meijer, Aggregation of Ureido-Pyrimidinone Supramolecular Thermoplastic Elastomers into Nanofibers: A Kinetic Analysis, Macromolecules 44(17) (2011) 6776-6784.

[16] R.A. Koevoets, R.M. Versteegen, H. Kooijman, A.L. Spek, R.P. Sijbesma, E.W. Meijer, Molecular Recognition in a Thermoplastic Elastomer, Journal of the American Chemical Society 127(9) (2005) 2999-3003.

[17] C. Hilger, R. Stadler, New multiphase architecture from statistical copolymers by cooperative hydrogen bond formation, Macromolecules 23(7) (1990) 2095-2097.

[18] C. Hilger, R. Stadler, Cooperative structure formation by directed noncovalent interactions in an unpolar polymer matrix. 7. Differential scanning calorimetry and small-angle x-ray scattering, Macromolecules 25(24) (1992) 6670-6680.

[19] R. Chang, Y. Huang, G. Shan, Y. Bao, X. Yun, T. Dong, P. Pan, Alternating poly(lactic acid)/poly(ethylene-co-butylene) supramolecular multiblock copolymers with tunable shape memory and self-healing properties, Polymer Chemistry 6(32) (2015) 5899-5910.

[20] J.C. Wittmann, B. Lotz, Epitaxial crystallization of monoclinic and orthorhombic polyethylene phases, Polymer 30(1) (1989) 27-34.

[21] L. Fontana, D.Q. Vinh, M. Santoro, S. Scandolo, F.A. Gorelli, R. Bini, M. Hanfland, High-pressure crystalline polyethylene studied by x-ray diffraction and ab initio simulations, Physical Review B 75(17) (2007) 174112.

[22] T. Seto, T. Hara, K. Tanaka, Phase Transformation and Deformation Processes in Oriented Polyethylene, Japanese Journal of Applied Physics 7(1) (1968) 31-42.

[23] V.F. Holland, Dislocations in Polyethylene Single Crystals, Journal of Applied Physics 35(11) (1964) 3235-3241.

[24] Y. Takahashi, T. Ishida, M. Furusaka, Monoclinic-to-orthorhombic transformation in polyethylene, Journal of Polymer Science Part B: Polymer Physics 26(11) (1988) 2267-2277.

[25] B.J.B. Folmer, R.P. Sijbesma, R.M. Versteegen, J.A.J. van der Rijt, E.W. Meijer, Supramolecular Polymer Materials: Chain Extension of Telechelic Polymers Using a Reactive Hydrogen-Bonding Synthon, Advanced Materials 12(12) (2000) 874-878.

[26] B. Wunderlich, C.M. Cormier, Heat of fusion of polyethylene, Journal of Polymer Science Part A-2: Polymer Physics 5(5) (1967) 987-988.

[27] L. Mandelkern, J.G. Fatou, R. Denison, J. Justin, A calorimetric study of the fusion of molecular weight fractions of linear polythylene (1), Journal of Polymer Science Part B: Polymer Letters 3(10) (1965) 803-807.

[28] J. Ilavsky, P.R. Jemian, Irena: tool suite for modeling and analysis of small-angle scattering, Journal of Applied Crystallography 42(2) (2009) 347-353.

[29] G. Beaucage, Small-Angle Scattering from Polymeric Mass Fractals of Arbitrary Mass-Fractal Dimension, Journal of Applied Crystallography 29(2) (1996) 134-146.

[30] G. Beaucage, D.W. Schaefer, Structural studies of complex systems using small-angle scattering: a unified Guinier/power-law approach, Journal of Non-Crystalline Solids 172-174 (1994) 797-805.

[31] K.E. Russell, B.K. Hunter, R.D. Heyding, Monoclinic polyethylene revisited, Polymer 38(6) (1997) 1409-1414.

[32] W. Hu, E.B. Sirota, Monoclinic Crystallites in Ethylene Copolymers Detected by Solid-State NMR and X-ray Diffraction, Macromolecules 36(14) (2003) 5144-5149.

[33] Z. Su, Y. Zhao, Y. Xu, X. Zhang, S. Zhu, D. Wang, J. Wu, C.C. Han, D. Xu, Spectroscopic Investigation of the Polymorphism and Side Group Location of Ethylene Copolymers, Macromolecules 37(9) (2004) 3249-3256.

[34] H.-J. Luo, Q. Chen, G. Yang, D. Xu, Phase structure of ethylene-dimethylaminoethyl methacrylate copolymers and its relation to comonomer content as studied by solid-state high-resolution 13C n.m.r. spectroscopy, Polymer 39(4) (1998) 943-947.

[35] D.K. Hohl, S. Balog, C. Cappelletti, F. Karasu, C. Weder, Crystallizable Supramolecular Polymers: Binding Motif and Processing Matter, Macromolecules 53(20) (2020) 9086-9096.

[36] E. Boz, K.B. Wagener, A. Ghosal, R. Fu, R.G. Alamo, Synthesis and Crystallization of Precision ADMET Polyolefins Containing Halogens, Macromolecules 39(13) (2006) 4437-4447.

[37] D.J.M. van Beek, M.A.J. Gillissen, B.A.C. van As, A.R.A. Palmans, R.P. Sijbesma, Supramolecular Copolyesters with Tunable Properties, Macromolecules 40(17) (2007) 6340-6348.

[38] G.M. Stack, L. Mandelkern, I.G. Voigt-Martin, Crystallization, melting, and morphology of low molecular weight polyethylene fractions, Macromolecules 17(3) (1984) 321-331.

[39] A. Alizadeh, L. Richardson, J. Xu, S. McCartney, H. Marand, Y.W. Cheung, S. Chum, Influence of Structural and Topological Constraints on the Crystallization and Melting Behavior of Polymers. 1. Ethylene/1-Octene Copolymers, Macromolecules 32(19) (1999) 6221-6235.

[40] R. Androsch, M.L. Di Lorenzo, C. Schick, B. Wunderlich, Mesophases in polyethylene, polypropylene, and poly(1-butene), Polymer 51(21) (2010) 4639-4662.

[41] B. Crist, SAXS Studies of Polymer Melting: Models for Surface Melting, Sequential Melting, and Stack Melting, Macromolecules 36(13) (2003) 4880-4890.

[42] L. Le Bras, R. Berthin, I. Hamdi, M. Louati, S. Aloïse, M. Takeshita, C. Adamo, A. Perrier, Understanding the properties of dithienylethenes functionalized for supramolecular self-assembly: a molecular modeling study, Physical Chemistry Chemical Physics 22(13) (2020) 6942-6952.

[43] I. Hamdi, G. Buntinx, O. Poizat, A. Perrier, L. Le Bras, S. Delbaere, S. Barrau, M. Louati, M. Takeshita, K. Tokushige, M. Takao, S. Aloïse, Excited-State Dynamics of Dithienylethenes Functionalized for Self-Supramolecular Assembly, The Journal of Physical Chemistry A 122(14) (2018) 3572-3582.

Graphical Abstract